

Third-Body-Driven vs. One-Impulse Plane Changes¹

B.F. Villac² and D.J. Scheeres³

Abstract

Third-body-driven plane changes, i.e., plane change maneuvers that use third-body forces to reduce the cost of the maneuver, are compared to one-impulse plane changes, the only classical approach still applicable in environments strongly perturbed by a third body. It is shown in particular that, although having inherent restrictions, the realizable range of third-body-driven plane changes covers a wide range of initial conditions and is closely related to the existence of $\pm 180^\circ$ plane changes. The question of the optimal method for performing a given plane change with given initial conditions and the maximal cost of such transfers are addressed semi-analytically to help in the design of such maneuvers in third-body-perturbed environments. It is found that third-body-driven plane changes are more fuel efficient than one-impulse maneuvers for plane changes values larger than $\sim 45^\circ$ (exact value depending on the case considered). The examples of Mars and Callisto orbiters have been used to illustrate the theory.

Introduction

The classical approach to orbit transfers is to assume an underlying two-body model and investigate the different ways of transferring from one conic orbit to another [1]. Between two successive impulsive burns, the orbit is characterized by a set of constant values, the orbital elements, which allow us to decide, most often analytically, about the optimality of a given transfer. However, when perturbations occur, this classical approach breaks down due to more complex dynamics that can result in large orbital element changes from one periapsis passage to the next [2]. Placing a spacecraft on a transfer trajectory prescribed by a two-body model may result in an impact with the primary before reaching the next periapsis passage, and the ΔV estimates thus obtained do not necessarily yield useful information. However, in transfers such as weak stability boundary ballistic capture [3] or insertions into halo orbits [4], using invariant manifold theory shows that these

¹First presented at the 2003 AAS/AIAA Astrodynamics Specialist conference in Big Sky, Montana. Paper AAS 03-519.

²Corresponding author. Assistant Professor, Department of Mechanical and Aerospace engineering, University of California, Irvine, CA. E-mail: bvillac@uci.edu.

³Professor, A. Richard Seebass Endowed Chair, Department of Aerospace Engineering, Colorado University, Boulder, CO. E-mail: scheeres@colorado.edu.

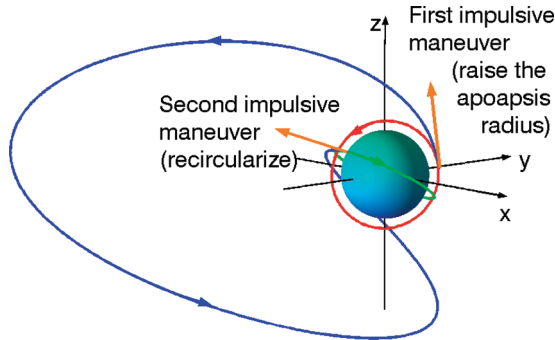


FIG. 1. Third-Body Driven Plane Change.

perturbed dynamics can be used effectively for control purposes, reducing, in some cases drastically, the total cost of the transfers.

In reference [5], third-body perturbations have been used to perform plane change maneuvers at reduced cost over the classical approaches. The resulting new class of plane change maneuvers, third-body–driven plane changes, are similar to the classic bi-elliptic plane change maneuvers with the apoapsis maneuvers replaced by the cost free action of the third-body perturbations (see Fig. 1). Although inherently restricted by the underlying dynamics (modeled by Hill’s problem), these transfers have been shown to be optimal over the one-impulse plane changes (the only classical maneuver still applicable in these perturbed environments) for a large range of initial conditions [6].

This article reviews and extends these results while applying the theory to the case of Mars and Callisto orbiters (~ 200 -km altitude). In particular, the allowable range of third-body–driven plane changes is computed and related to the existence of $\pm 180^\circ$ plane changes. The question of optimality of these transfers over one-impulse maneuvers is answered semi-analytically and an upper bound on the cost of such transfers is presented.

Third-Body–Driven Plane Changes

The plane change problem considered consists of finding a trajectory that transfers a spacecraft from an initial circular orbit of given radius r_0 and inclination i to a final circular orbit with same radius r_0 but with a different inclination, $i + \Delta i$. Classically, the methods used for performing the maneuvers consist of one-impulse, bi-elliptic, parabolic or general three-impulse maneuvers [1], which have only been analyzed in a two-body framework. Among these methods, only the one-impulse maneuver, which consists of rotating the velocity vector of the initial circular orbit at one of the nodes, is still applicable in strongly perturbed environments. Indeed, the remaining methods involve a transfer trajectory with a large apoapsis radius (“infinity” for plane changes larger than 60°) so that the third-body perturbations, which increase linearly with distance from the primary, induce large changes in the orbital elements over the transfer (and possibly cancel the effect of the classical apoapsis burn) and the two-body assumption does not hold anymore. The presence of third-body perturbations, however, can be used to one’s advantage and improve over the classic analysis of plane change maneuvers, as has been shown in reference [5]. This section reviews the model used to represent the

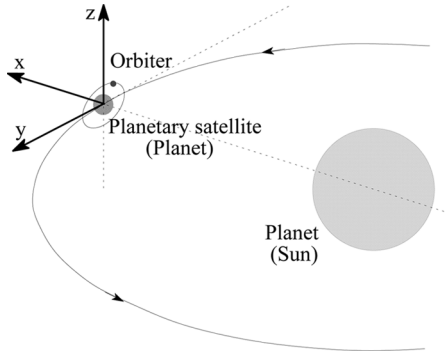


FIG. 2. Geometry of Hill's Problem in the Case of an Orbiter.

perturbed orbital environment and the basic geometry and results about third-body driven plane changes.

Hill's Problem

The Hill's problem is an approximate model derived from the three-body model that represents the motion of two close, gravitationally interacting small masses, as perturbed by a larger, distant body. This model is well suited to represent the motion of an orbiter around a primary (planet or planetary satellite) as perturbed by a massive body (Sun or giant planet, respectively). Although arbitrary elliptic orbits of the primary can be considered, we assume here that the primary moves in a circular orbit around the massive body. As compared to the more widely used circular restricted three-body problem, Hill's problem has the advantage of a simple and parameterless set of equations with the presence of symmetries that simplify the numerical computations [7].

Hill's problem is formulated in a rotating frame with angular velocity N (corresponding to the mean motion of the primary around the disturbing body in the case of the orbiter problem) centered at the primary, as shown in Fig. 2. Denoting the gravitational parameter of the primary as μ , one can define length and time scales, l and τ , respectively, as

$$l = \left(\frac{\mu}{N^2} \right)^{1/3} \quad \text{and} \quad \tau = \frac{1}{N}$$

so that the equations of motion are expressed in parameterless form as

$$\begin{cases} \ddot{x} - 2\dot{y} &= -\frac{x}{r^3} + 3x \\ \ddot{y} + 2\dot{x} &= -\frac{y}{r^3} \\ \ddot{z} &= -\frac{z}{r^3} - z \end{cases} \quad (1)$$

where dots represent time derivatives, x , y , and z are the coordinates of the position vector of the spacecraft (in the rotating frame defined above), and r is the Euclidean norm of that position vector.

In this work, all the computations will be performed in this normalized setting (and may thus be applied to a range of physical systems by a simple scaling).

TABLE 1. Numerical Parameters for Mars and Callisto

Primary	μ (km ³ /s ²)	N (rad/s)	l (km)	τ (hr)	Radius (km)	Normalized radius	ΔV scale (m/s)
Mars	42832	1.058e-7	1084027.7	2623.82	3397	0.00313	114.7
Callisto	7171	4.357e-6	72283.6	63.75	2400	0.0332	314.9

However, some dimensional results will be given for the cases of Mars and Callisto orbiters to illustrate the theory. Table 1 summarizes the numerical values used for these primaries. Notably, the case of an orbiter in a ~ 212.8 km altitude has been used for the case of Mars, whereas a 166.0 km altitude orbiter has been used for the case of Callisto. These correspond to normalized radii of 0.00333 and 0.0355, respectively. These examples are representative of two different realms of dynamics and are separated by an order of magnitude in normalized radii. Note that the last column of the table (l/τ) allows for conversion of the ΔV values obtained in the normalized unit system to the corresponding physical units. In particular, a normalized ΔV of 1 represents a lesser change in velocity at Mars than at Callisto.

Note also that Hill's equations consist of a Kepler problem in a rotating frame with an additional linear term representing the third-body perturbation. Thus, when close to the primary, the perturbation tends to zero as compared to the Keplerian term, and the low-altitude dynamics can be represented for several orbits by Keplerian motion in a rotating frame. Averaging theory indicates that this approximation is valid for a normalized radius less than ≈ 0.2 [7, 8]. Above this radius, the dynamics become strongly non-Keplerian and at $x = \pm(1/3)^{1/3} \approx 0.69$, the perturbing and Keplerian terms cancel each other, resulting in the equilibrium solutions that correspond to the libration points, L_1 and L_2 .

A first integral of the equations of motion, known as the Jacobi constant, is expressed in the inertial space as

$$J = \frac{1}{2} V^2 - \frac{1}{r} - G \cos i + \frac{1}{2} r^2 - \frac{3}{2} x^2 \quad (2)$$

where r denotes the magnitude of the position vector, V represents the inertial velocity, G is the magnitude of the angular momentum, and i is the inclination. This expression will be used to derive estimates of the cost of the third-body–driven plane changes in the section Optimal Plane Change Strategies.

Finally from equation (1), it can easily be checked that the equatorial plane is invariant under the flow and that the symmetries with respect to the origin (both in the spatial and planar case) leave the equations invariant. That is, the dynamics are invariant with respect to shifts of $m\pi$, $m \in \mathbf{Z}$, in longitude of ascending node, Ω , and argument of periapsis, ω . Thus, numerical investigations need only be performed on the “reduced” torus-space $T^2 = [0 \pi] \times [0 \pi]$.

Third-Body–Driven Plane Changes

Before detailing the steps at the basis of third-body–driven plane changes, we should like to clarify two technicalities. On one hand, because at low altitudes, quasi-circular motion exists and can be approximated by a Keplerian motion in a rotating frame (i.e., with a precession of the nodes) for several spacecraft orbits, the plane change problem in a third-body–perturbed environment still makes sense.

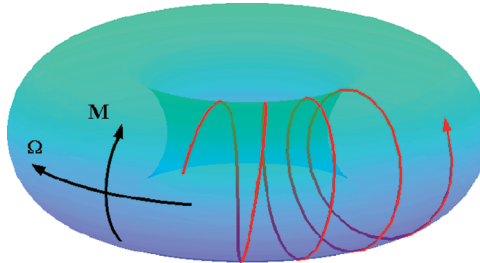


FIG. 3. Motion of a Spacecraft on a Circular Orbit as Viewed in the (M, Ω) -Torus Space.

That is, one can talk about an initial and final “circular orbit” and transfer between them. On the other hand, to represent the dynamics along transfer trajectories whose apoapsis are far from the central body, one cannot neglect the influence of the perturbing body, and Hill’s problem should thus be used. Different choices of ω and Ω at the periapsis of the transfer trajectory (i.e., the orientation of this trajectory with respect to the disturbing body) lead to completely different transfers.

Third-body–driven plane changes are therefore achieved by placing the spacecraft on a carefully chosen transfer trajectory whose initial orientation ensures that the plane change is performed without any apoapsis burn, thus resembling the classical bi-elliptic maneuvers with the apoapsis maneuver suppressed by the use of the third-body perturbations. That is, from the initial circular orbit, one performs a first tangential maneuver to place the spacecraft along a transfer trajectory whose orientation allows the perturbing body to perform a plane change while leaving the periapsis radius unchanged. At the next periapsis (after one orbit), one can then simply place the spacecraft on the final circular orbit with another tangential burn, as was illustrated in Fig. 1. Although the strategy can certainly be generalized by including nontangential burns and additional apoapsis maneuvers, the above strategy is simpler to implement and analyze (lower dimensional trade-space), while already providing significant savings over one-impulse maneuvers. In a third-body framework, these third-body–driven plane-change maneuvers play the same role as the bi-elliptic transfers and clarify the link between the underlying dynamics and the maneuver parameters. This paper thus focuses solely on this approach.

The timing of the first maneuver can be understood by taking a closer look at the dynamics on the initial circular orbit. When the spacecraft moves along the initial, low altitude, circular orbit, the mean anomaly, M , and the longitude of the ascending node, Ω , are (in the Keplerian approximation used) linear functions of time and can be represented as a line wrapping in the (M, Ω) -torus space (all the other orbital elements remaining fixed during the motion by our approximation of circular motion), as illustrated in Fig. 3. Inasmuch as the slope of this line will almost certainly be irrational, any value of M and Ω can be approximated to any degree of accuracy by waiting for a sufficiently long time. The timing of a tangential impulsive maneuver will thus allow control of the orientation of the transfer trajectory relative to the Europa–Jupiter line. In practice, any value of M and Ω can be approximated to within $\sim 1^\circ$ after a few spacecraft orbits. For example, in the case of a Mars orbiter, Ω varies by 0.04° during a spacecraft orbit (~ 200 -km orbiter) so that any value of (M, Ω) can be reached to within 0.02° .

accuracy. Similarly, in the case of the Callisto orbiter, any value of (M, Ω) can be approximated to within 1.23° .

The effect of a tangential maneuver on the initial circular orbit then consists of fixing the orientation of the transfer relative to the perturbing body. More precisely, a tangential impulsive maneuver at any point of this initial circular orbit will place the spacecraft at the periapsis of a transfer trajectory, the orbital elements of which are determined using the following correspondences

Initial, circular orbit	Transfer trajectory	
r_0	→	r_p
ΔV	→	$r_a(\Delta V)$
i	→	i
$\Omega = -Nt$	→	Ω
$M = nt$	→	ω

(3)

where $n = \sqrt{1/r_0}$ represents the mean motion of the spacecraft on the initial circular orbit, whereas r_p and r_a are the periapsis and apoapsis radii of the transfer trajectory when evaluated just after this first burn.⁴

Note in particular that ω and Ω are directly related to the value of M and Ω of the initial circular orbit, i.e., time.⁵ Thus, from the previous discussion, any value of (ω, M) of the transfer trajectory can be targeted by timing this first maneuver.

The existence of third-body–driven plane changes is ensured by the existence of some values of (ω, Ω) resulting in a zero change in periapsis radius at the next periapsis passage of the transfer trajectory, while having a nonzero change in inclination (and, in fact, this change can be rather large, as we will see below). Thus, choosing such values for ω and Ω , one only need perform a recircularization (tangential) burn at the next periapsis to complete a plane change maneuver. Mathematically, the choice of ω and Ω amounts to solving the following non-convex optimization problem

$$\max_{(\omega, \Omega) \in T^2} \Delta i_{(\omega, \Omega)} \quad \text{subject to} \quad \Delta r_{p(\omega, \Omega)} = 0 \quad (4)$$

where the notation Δ represents a change between successive periapsis passages.⁶ This procedure can be visualized by computing the changes Δr_p and Δi for each value of ω and Ω and plotting the intersection of the curves $\Delta r_p(\omega, \Omega) = 0$ with the level curves of Δi . This is shown in Fig. 4 where the spacecraft’s initial circular orbit has been also represented (owing to the correspondences of equation (3)). Finally, we note that Fig. 1, used to illustrate the geometry of the third-body–driven plane changes, corresponds indeed to an actual transfer computed with this method.

⁴The value of r_a is directly related to the size of ΔV , whereas r_p is independent of the magnitude of the maneuver (as long as the maneuver is performed in the direction of the initial circular velocity). This is emphasized by the notation $r_a(\Delta V)$.

⁵In the correspondences, given in equation (3), the time is assumed to be counted relative to an epoch when the longitude of the ascending node of the initial circular orbit is zero in Hill’s frame (these events occur once per orbit of the primary around the perturbing body). More generally, one could define the longitude of the ascending node of the initial circular orbit at a given epoch t_0 to be Ω_0 , so that the longitude of the ascending node as a function of time would then be given as $\Omega = \Omega_0 - N(t - t_0)$.

⁶That is, $\Delta x = x(\text{final periapsis}) - x(\text{initial periapsis})$.

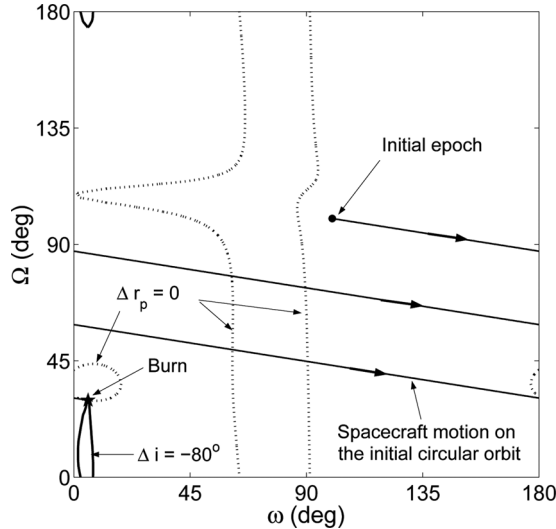


FIG. 4. A Geometric View of Third-Body-Driven Plane Changes.

Dynamical Restrictions

The previous method allows us to show that third-body–driven plane changes are less expensive than one-impulse maneuvers for sufficiently large plane-change values. However, the invariance of the equatorial plane in Hill’s problem restricts the range of third-body–driven plane changes realizable. Transfer from a non-equatorial to an equatorial trajectory is not possible using this method, and one-impulse maneuvers must be used to perform such transfers.

Besides the limitations on the extrema values of the solution of equation (4), this restriction manifests itself also in the topology of this optimization problem. More precisely, the extrema of plane change may be located on two disconnected components of the level curves $\Delta r_p(\omega, \Omega) = 0$ and not all the plane-change values in between these two extrema may be possible. Figure 5 shows a situation where there are several disconnected zero level curves of Δr_p , but the global Δi extrema are located on a single component. Thus, in this case, any values of plane change between -80.9° and $+79.2^\circ$ are possible. These global extrema may however be on different components for different values of initial inclination, and a gap in the values of realizable plane change then results. For example, for equatorial orbits mentioned above, although the maxima and minima plane changes may be 180° and 0° , respectively, plane change values in the range $0^\circ < \Delta i < 180^\circ$ are not feasible with the two-impulse strategy considered in this article.

Therefore, numerically, one has to compute the extrema of plane change on each connected component of $\Delta r_p(\omega, \Omega) = 0$ to determine the range of third-body–driven plane changes. These computations have been performed for different values of apoapsis radius in the case of Mars and Callisto, as shown in Fig. 6. We can see from these graphs that the third-body–driven plane-change range increases significantly with apoapsis radius, r_a , until the $\pm 180^\circ$ plane changes appear to be possible. In this case, the range still increases with r_a but very slowly. Also, we can observe that negative values of plane change are larger than positive values (globally) for any given r_a . In particular, although -180° plane change are possible for planetary satellites (here

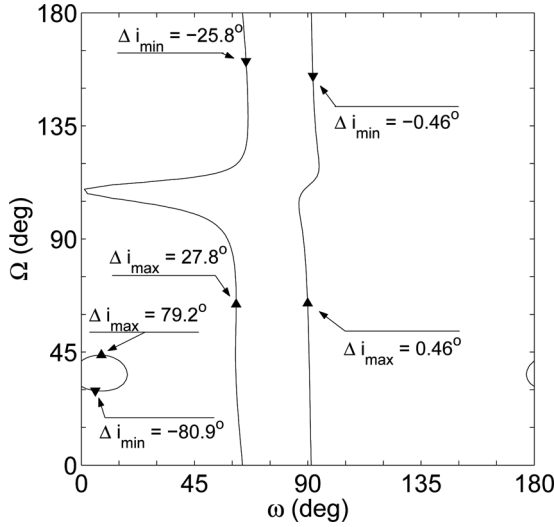


FIG. 5. $\Delta r_p = 0$ Line for $r_p = 0.003$, $r_a = 0.5$, and $i = 90^\circ$.

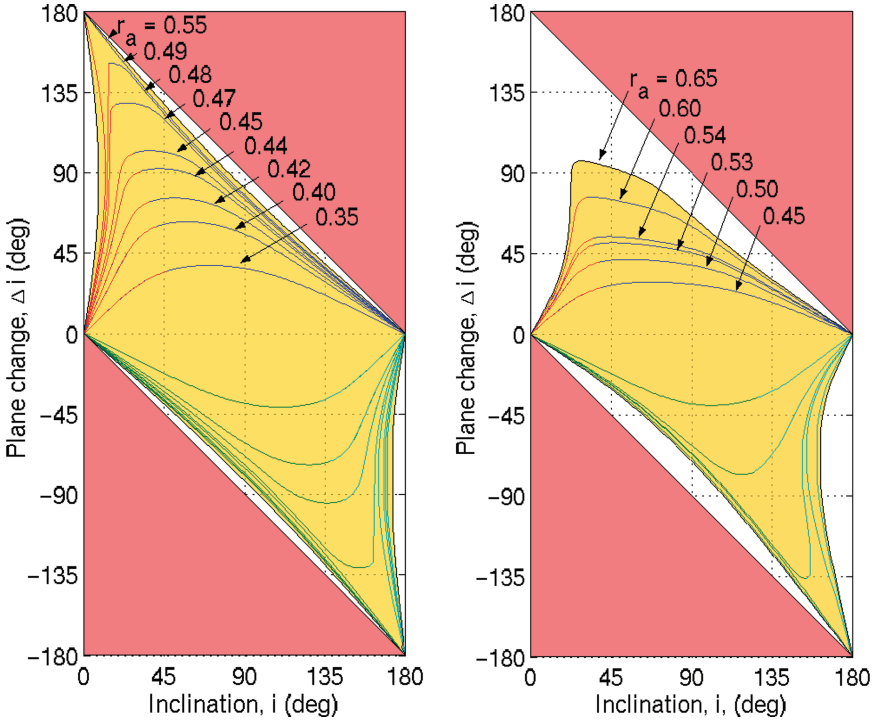


FIG. 6. Range of Possible Third-Body-Driven Plane Changes in the Case of the Mars (Left) and Callisto (Right) Orbiters.

Callisto), $+180^\circ$ plane changes are not necessarily possible for reasonable values of r_a , showing that the potential advantages of third-body–driven plane changes should be more apparent for negative plane-change values.

These results indicate that the maximal range of third-body–driven plane changes is well approximated by the range obtained when $\pm 180^\circ$ plane changes are realizable.

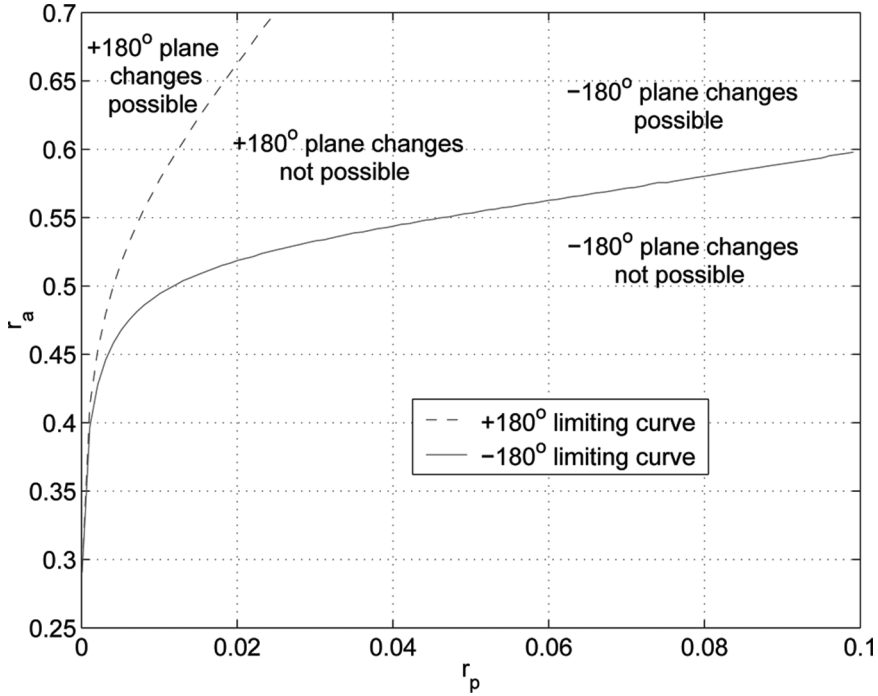


FIG. 7. Limits of Existence for $\pm 180^\circ$ Plane Changes.

These “change of direction” transfers only involve the planar dynamics, and their domain of existence can be computed as a function of the initial conditions r_p and r_a . The results of these computations are shown in Fig. 7. We note that these transfers correspond to nearly zero angular momentum trajectories when $r_p \rightarrow 0$. Even if their possibility appears as a bifurcation in the planar case, Fig. 6 shows that these transfers follow from the increasing variations of the range of third-body–driven plane changes with apoapsis radius when viewed in the three-dimensional problem.

Optimal Plane Change Strategy

The previous discussion shows that, for equatorial or near-equatorial orbits, one-impulse maneuvers must be used to perform plane-change maneuvers. However, when feasible, third-body–driven plane changes may result in significant fuel savings when compared to one-impulse maneuvers [5]. This section makes explicit the trade-offs between these strategies by deriving analytical estimates of the cost of the third-body–driven plane changes.

Estimate of the Cost of Third-body-Driven Plane Changes

We have seen in the previous section that Hill’s problem has a first integral of motion, J . This integral depends on the position and speed of the spacecraft, and the main contribution due to the position in the case of low altitudes depends on the magnitude of the radius vector, r . Thus, in the case of third-body–driven plane-change maneuvers, where both impulsive burns are made at a given low altitude, the Jacobi constant can be used to obtain an accurate estimate of the cost of the maneuver. More precisely, because J is constant along the transfer trajectory, its difference in value between the two successive periapsis passages (initial and

final) of the transfer trajectory is zero. Hence, using equation (2) and denoting the initial and final periapsis by the subscripts 1 and 2, respectively, one obtains

$$\Delta J = J_2 - J_1 = 0 = \frac{1}{2}(V_2^2 - V_1^2) - r_p V_2 \cos(i + \Delta i) + r_p V_1 \cos(i) - \frac{3}{2}(x_2^2 - x_1^2) \quad (5)$$

The term $c = \frac{3}{2}(x_2^2 - x_1^2)$ can be bounded independently of ω and Ω

$$-\frac{3}{2}r_p^2 \cos^2(i) \leq c \leq \frac{3}{2}r_p^2 \cos^2(i + \Delta i)$$

showing its smallness for low initial and final altitudes.

Now, equation (5) represents a quadratic form in V_2 and can be solved explicitly⁷

$$V_2 = r_p \cos(i + \Delta i) + \sqrt{r_p^2 \cos^2(i + \Delta i) + V_1^2 - 2r_p V_1 \cos(i) + 2c}$$

so that, upon substituting the bound on c , one obtains a bound on V_2

$$V_2^- \leq V_2 \leq V_2^+ \quad (6)$$

where

$$\begin{cases} V_2^- = r_p \cos(i + \Delta i) + \sqrt{r_p^2 \cos^2(i + \Delta i) - 3r_p^2 \cos^2(i) + V_1^2 - 2r_p V_1 \cos(i)} \\ V_2^+ = r_p \cos(i + \Delta i) + \sqrt{4r_p^2 \cos^2(i + \Delta i) + V_1^2 - 2r_p V_1 \cos(i)} \end{cases}$$

Note that, because the first impulse used to raise the apoapsis of the transfer trajectory is tangential, V_1 only depends on r_p and r_a

$$V_1 = \alpha V_{lc}; \quad \alpha = \sqrt{\frac{2r_a/r_p}{1 + r_a/r_p}}$$

where $V_{lc} = \sqrt{1/r_p}$ represents the local circular speed of the spacecraft.⁸ Thus, the bounds on V_2 (equation (6)) only depend on r_p , r_a , i , and Δi and, because the cost of the third-body-driven plane changes is expressed as

$$\Delta V = V_1 + V_2 - 2V_{lc}$$

one obtains a bound on this cost, independently of ω and Ω

$$\Delta V^- \leq \Delta V \leq \Delta V^+ \quad (7)$$

where $\Delta V^\pm = V_1 + V_2^\pm - 2V_{lc}$.

Note also that the error made when using this bound (i.e., $\Delta V^+ - \Delta V^-$) is smaller than $2\sqrt{\frac{3}{2}}r_p$,⁹ so that the estimate $\tilde{\Delta V} = (\Delta V^- + \Delta V^+)/2$ has an accuracy of $\pm\sqrt{\frac{3}{2}}r_p$. For low-altitude orbiters, this may be sufficient for mission preliminary analysis. For example, in the case of the 200-km altitude Mars orbiter, this bound is accurate to within $\pm 0.47 \text{ m}\cdot\text{s}^{-1}$ and, in the case of the Callisto orbiter, the accuracy is $\pm 13.7 \text{ m}\cdot\text{s}^{-1}$ (both cases represent less than 1% error on the actual cost).

⁷Only one of the solutions can be shown to be real.

⁸Recall that, in the normalized Hill's problem, the gravitational parameter of the primary has a value of 1, so that $\sqrt{1/r_p}$ is indeed homogeneous to a velocity.

⁹Indeed, from equation (6), $V_s^+ = \sqrt{(V_2^-)^2 + 3r_p^2(\cos^2(i) + \cos^2(i + \Delta i))} \leq \sqrt{(V_2^-)^2 + 6r_p^2} \leq V_2^- + \sqrt{6}r_p$. Note that, even though the bound appears to be homogeneous to a distance, in the normalized setting where the gravitational and angular frequency of the frame are both equal to one, this bound is really homogeneous to a velocity.

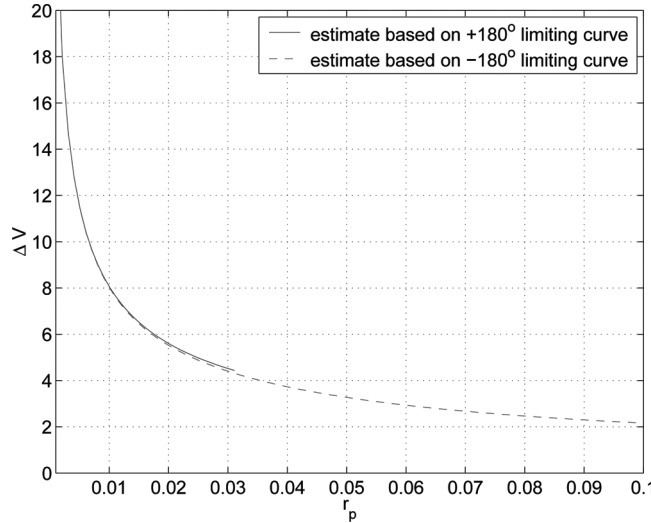


FIG. 8. Maximal Cost of Third-Body-Driven Plane Changes as a Function of Initial Periapsis Radius.

This result does not give a complete picture of the problem because we don't know a priori what value of plane change Δi is realizable for a given apoapsis radius. However, one can use the previous numerical computations of the ranges to obtain an upper bound on the cost of these transfers. More precisely, we note that the dependence on i and Δi in the above cost estimate is small and can be bounded

$$\Delta V \leq V_{lc} \left\{ \alpha - 2 + r_p^{3/2} + \sqrt{(\alpha + r_p^{3/2})^2 + 3r_p^{3/2}} \right\} \quad (8)$$

Now, because the maximal range of third-body–driven plane changes is approximated by the range obtained at the limit of existence of $\pm 180^\circ$ plane changes, one can evaluate equation (8) along the curves shown in Fig. 7 to obtain a maximal cost estimate. This is shown on Fig. 8. In the case of a planetary Moon orbiter, the estimate is based only on the limit of existence of -180° plane changes.

In the case of the Mars orbiter, this cost estimate is on the order of $1629.6 \text{ m}\cdot\text{s}^{-1}$ (based on the existence of $\pm 180^\circ$ plane change limit, i.e., $r_a \approx 0.49$), whereas in the case of the Callisto orbiter, this estimate is only $1258.6 \text{ m}\cdot\text{s}^{-1}$ (based on the existence of -180° plane change limit, $r_a \approx 0.539$). These results illustrate the difference, already observed in the second section, between the case of planetary and planetary satellite orbiters. In the case of a planetary orbiter, this upper estimate is very close to the cost of a parabolic transfer ($1646.6 \text{ m}\cdot\text{s}^{-1}$), thus seemingly not improving on the two-body analysis. The analysis performed, however, indicates that the implementation of the plane change must be performed more carefully than indicated by the two-body problem analysis, i.e., the timing of the maneuver does matter. In the case of planetary satellite orbiters, the use of the third-body forces is even more apparent, especially for the negative values of plane change. In the case of Callisto, the savings (as compared to the parabolic estimates) are on the order of $126 \text{ m}\cdot\text{s}^{-1}$. These savings increase with the magnitude of the normalized radius of the planetary satellite. Even though these savings are significant, the results obtained still indicate that large plane-change maneuvers are expensive, even when aided by third-body perturbations.

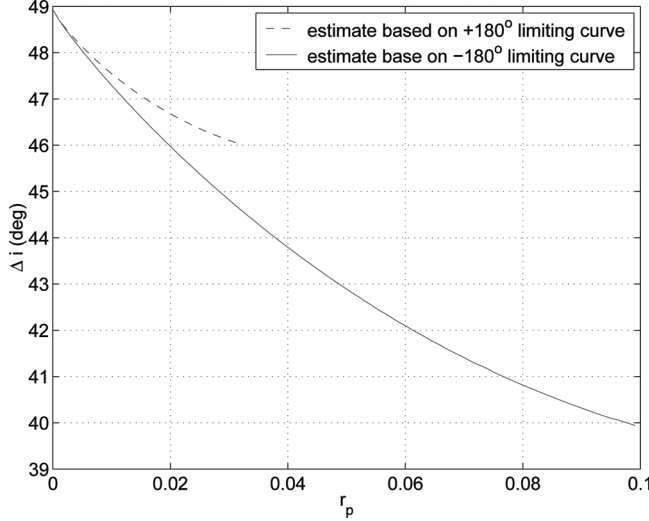


FIG. 9. Optimality Limit Between One-Impulse and Third-Body-Driven Plane Changes.

Limit of Optimality

Using the above cost estimate, an approximation to the limit of optimality between one-impulse and third-body-driven plane changes can be derived. Indeed, because the cost of one-impulse maneuvers is known

$$\Delta V_0 = 2V_{lc} \sin\left(\frac{|\Delta i|}{2}\right) \quad (9)$$

and the range of third-body-driven plane changes increases with r_a , we see that third-body-driven plane changes will be cheaper than one-impulse maneuvers, at least when

$$\Delta V^+(r_{a_{max}}) \leq \Delta V_0$$

where $r_{a_{max}}$ is obtained from the limits shown in Fig. 7. As shown previously, one can bound the small dependence on i and Δi in ΔV^+ to obtain an explicit upper bound on the optimality limit

$$|\Delta i| \geq 2 \arcsin\left\{\frac{\alpha}{2} - 1 + \frac{r_p^{3/2}}{2} + \frac{1}{2} \sqrt{(\alpha + r_p^{3/2})^2 + 3r_p^{3/2}}\right\} \quad (10)$$

Evaluating this bound on the limiting curves for the existence of $\pm 180^\circ$ plane changes, one obtains the upper bound on the limit of optimality as shown on Fig. 9. That is, for plane-change values above the values shown, third-body-driven plane changes are cheaper than one-impulse maneuvers, when realizable. This bound is illustrated on the range plots for the cases of the Mars and Callisto orbiters, as shown on Fig. 10. Third-body-driven plane changes are cheaper than one-impulse plane changes in the region of realizable transfers that are outside the horizontal, shaded strip. Note that the graph corresponding to Callisto also includes the boundary of realizable transfers for a larger apoapsis radius ($r_a = 0.65$) to illustrate the conservative nature of the bound for Moon orbiters. In such cases, the range of realizable transfers can be larger than the one estimated from the limit of existence of

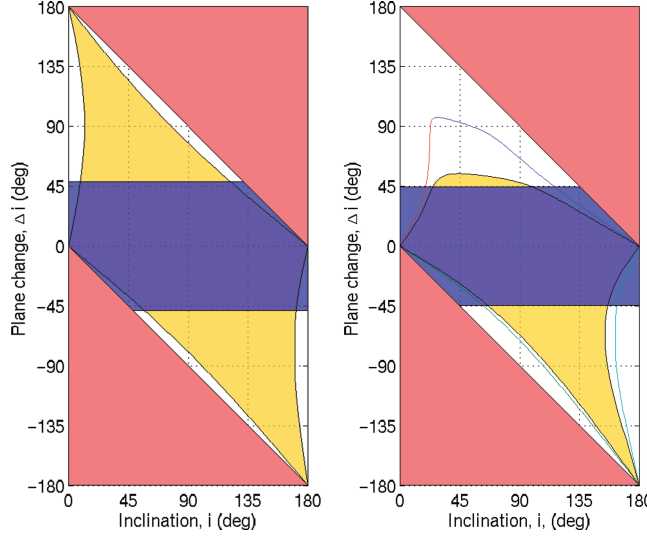


FIG. 10. Range of third-body–driven plane change with optimality limit in the case of the Mars (left) and Callisto (right) orbiters. The plot relative to Callisto also indicates the range of realizable third-body–driven plane changes for larger apoapsis radii ($r_a = 0.65$; see Fig. 6).

–180° transfers. The large region of non-realizable third-body–driven plane changes indicate the limitation of the approach investigated, and an apoapsis maneuver should thus be used to alleviate this limitation; a topic for future research.

As for the cost estimate, this result is very close to the limit of optimality between one-impulse and parabolic plane changes in the case of planetary orbiters (very small value of r_p , while being significantly smaller for the case of planetary satellite orbiters (larger r_p). In fact, because for small values of r_p the dependence on r_a is small, the bound obtained is very accurate. For example, in the case of the Mars orbiter, it can be checked that, for $r_a = 0.35$, one-impulse plane changes are always optimal and, because the variation of equation (10) with r_a (for larger values of r_a) is less than 0.5, we deduce that the bound obtained is accurate to within this value.

When r_p is larger, the bound obtained is a priori not so accurate, and a numerical correction may be necessary. Based upon the previous estimates, one can derive a quick algorithm to compute this limit. The underlying idea consists of comparing the Δi realized for a fixed ΔV , rather than comparing the ΔV at fixed Δi . This is possible because of the 1–1 relation between Δi and ΔV_0 on one hand, and the same monotonic dependence of Δi and ΔV on r_a for third-body–driven plane changes, on the other hand.

Thus, given an initial value Δi_0 , we have ΔV_0 given by equation (9). Then we can solve for r_a in $\Delta V^\pm(r_a) = \Delta V_0$, yielding two solutions r_a^\pm

$$r_a^\pm = \frac{(\alpha^\pm)^2 r_p}{2 - (\alpha^\pm)^2}; \quad \alpha^\pm = \frac{A^2 - B^\pm}{2V_{lc}(A - r_p \cos(i))} \quad (11)$$

where

$$\begin{cases} A = \Delta V_0 - r_p \cos(i + \Delta i) + 2V_{lc} \\ B^+ = 4r_p^{3/2} \cos^2(i + \Delta i); \quad B^- = r_p^2 \cos^2(i + \Delta i) - 3r_p^2 \cos^2(i) \end{cases}$$

Now, problem (4) can be solved numerically with r_a^\pm , resulting in Δi^\pm to be compared with Δi_0 .

Note that when $\Delta i^+ \leq \Delta i_0 \leq \Delta i^-$, one needs to solve exactly for ΔV to decide on the optimality by comparing with ΔV_0 . In practice, this case covers only a very thin strip of initial conditions and generally, the algorithm requires only solving problem (4) once or twice per initial conditions to settle the question.

Algorithm¹⁰

- Given r_p , i , and Δi_0 , solve for ΔV_0 using equation (9).
- Solve for r_a^\pm using the relation $\Delta V^\pm(r_a) = \Delta V_0$. (Note that $r_a^+ \leq r_a^-$).
- Solve the optimization problem (4) with r_p , r_a^\pm , i to obtain Δi^\pm . (Note that $\Delta i^+ \leq \Delta i^-$).
- compare:
 - If $(\Delta i_0 \geq \Delta i^-)$ then one-impulse transfers are optimal
 - If $(\Delta i_0 \leq \Delta i^+)$ then third-body–driven plane changes are optimal
 - If $(\Delta i^+ \leq \Delta i_0 \leq \Delta i^-)$ then use a dichotomy on r_a to solve exactly for ΔV

Applying this scheme to the case of Callisto, one can check that the analytical limit (10) is, at most, 1.5° above the numerically computed values.

Conclusion

The optimality of third-body–driven plane changes has been investigated. In particular, an analytical estimate of the limit of optimality has been derived, showing that third-body–driven plane changes are indeed less expensive than one-impulse maneuvers for a large domain of initial conditions and plane changes larger than $\approx 45^\circ$. Limitations of third-body–driven plane changes have been found because of the restrictions imposed by the natural dynamics. It seems that these limitations could be overcome by using artificial propulsion systems in conjunction with the use of the cost free, third-body forces, resulting in further optimality criteria. In particular, the general two-impulse case, that is the addition of small plane changes at each impulsive burn of the third-body–driven plane-change maneuvers considered in this article, should suffice for this purpose. This case can be analyzed along the same line followed in this article (the only difficulty being the numerical computation of $\partial \Delta V / \partial r_a$, which results in lengthy computational times). Note also that multiple revolution plane changes should be possible, extending the realizable range of third-body–driven plane changes. The criteria for optimality derived in this article would apply directly to this situation. However, the practical computation of such a transfer becomes more difficult as one has to restrict the domain of initial conditions (in ω and Ω) to avoid impact with the satellite (planet) before the desired periapsis is reached. Future research needs to be performed to find an answer to such possibilities.

References

- [1] CHOBOTOV, V.A. (ed.) *Orbital Mechanics*, 2nd edition, AIAA Education Series, 1996.
- [2] VILLAC, B.F., SCHEERES, D.J., D'AMARIO, L.A., and GUMAN, M.D. “The Effect of Tidal Forces in Orbit Transfers,” Paper AAS 01-247, Advances in the Astronautical

¹⁰Formulated here for $\Delta i_0 \geq 0$. A similar algorithm can be written for $\Delta i_0 \leq 0$.

- Sciences, Vol. 108, *AAS/AIAA Spaceflight Mechanics Meeting*, February 11–15, 2001, Santa Barbara, CA, 2001.
- [3] BELBRUNO, E. and MILLER, J. “Sun-Perturbed Earth-to-Moon Transfers with Ballistic Capture,” *Journal of Guidance, Control, and Dynamics*, Vol. 16, No.4, 1993, pp. 770–775.
 - [4] LO, M.W., WILLIAMS, B.G., BOLLMAN, W.E., HAN, D.S., HAHN, Y.S., BELL, J.L., HIRST, E.A., CORWIN, R.A., HONG, P.E., HOWELL, K.C., BARDEN, B., and WILSON, R. “Genesis Mission Designs”, *The Journal of the Astronautical Sciences*, Vol. 49, No.1, 2001, pp. 169–184.
 - [5] VILLAC, B.F. and SCHEERES, D.J. “A New Class of Optimal Plane Change Maneuvers,” *Journal of Guidance, Control, and Dynamics*, Vol. 26, No. 5, 2003, pp. 750–757.
 - [6] VILLAC, B.F. and SCHEERES, D.J. “Optimal Plane Changes Using 3rd Body Forces,” *Annals of the New York Academy of Sciences*, Vol. 1017, 2004, pp. 255–266.
 - [7] VILLAC, B.F. *Dynamics in the Hill Problem with Applications to Spacecraft Maneuvers*, Ph.D. Dissertation, The University of Michigan, 2003.
 - [8] SCHEERES, D.J., GUMAN, M.D., and VILLAC, B.F. “Stability Analysis of Planetary Satellite Orbiters: Application to the Europa Orbiter,” *Journal of Guidance, Control, and Dynamics*, vol. 24, No. 4, 2001, July-August.
 - [9] KOZLOV, V.V. and NEISHTADT, A.I. “Mathematical Aspects of Classical and Celestial Mechanics,” *Encyclopaedia of Mathematical Sciences, Dynamical Systems III*, 3rd edition, Springer-Verlag, Berlin and Heidelberg, 2006.